Journal of Membrane Science 525 (2017) 107–115

Contents lists available at ScienceDirect

Journal of Membrane Science

journal homepage: www.elsevier.com/locate/memsci

Hybrid membrane distillation-reverse electrodialysis electricity generation system to harvest low-grade thermal energy

Rui Long*, Baode Li, Zhichun Liu, Wei Liu*

School of Energy and Power Engineering, Huazhong University of Science and Technology, 1037 Luoyu Road, Wuhan 430074, China

ARTICLE INFO

Keywords:
Membrane distillation (MD)
Reverse electrodialysis (RED)
Heat engine
Low-grade heat harvesting

ABSTRACT

An alternative hybrid membrane-based electricity generation system that operates as a heat engine is presented to convert low-grade heat into electricity. This system consists of membrane distillation (MD), which absorbs thermal energy from the heat source and generates high concentrated salty stream, and reverse electrodialysis (RED), that converts the Gibbs free energy of mixing from the produced salty streams into electricity. The MD-RED system was simulated by considering both the heat and mass transfer characteristics in the thermal separation (MD) and electricity generation (RED) procedures with heat source temperature varying from 40 °C to 80 °C and the MD feed NaCl concentrations of 1.0, 2.0, 3.0, 4.0, and 5.0 mol/kg. The performance specifications, i.e. the mass recovery rate, specific heat duty, heat absorbed, and power output are systematically discussed, which are directly impacted by the relative MD permeate/feed solution flow rate. Results reveal that there exists an optimal relative permeate/feed solution flow rate leading to the maximum electrical efficiency of the proposed MD-RED system under given operating temperatures for different MD feed NaCl concentrations. Moreover, approximate analytic expressions of the power output and the electrical efficiency have been deduced. Larger MD feed NaCl concentration induces greater electrical efficiency. The electrical efficiency of the hybrid MD-RED system reaches 1.15% operating between 20 and 60 °C with the MD feed NaCl concentration of 5 mol/kg, which indicates its potential application for low-grad heat harvesting.

1. Introduction

As the fast growing number of the global human beings, the energy supply faces serious challenges to meet the urging demands, along with the depletion of fossil fuels, from whose combustion environment suffers much [1]. Low-grade waste heat recovery and utilization of clean and renewable energy offer alternative ways to relieve such problems [2]. Every year, a huge amount of thermal energy is directly evacuated to the surroundings, or is just cooled down by refrigeration systems, most of which possess a relative high temperature, and could be further utilized [3]. Waste heat above 80 °C can be directly converted to useful work by using the organic Rankin cycle or the Kalina cycle [4–6], however for temperature below 80 °C, there are no practical technologies with satisfied efficiency to convert the low-grad waste heat into electricity. Efforts have been devoted to developing high efficiency heat convector devices and technologies to harvest low temperature thermal energy [7–9].

Pioneered by the previous study on extracting work from waters with different sanities [10], such technologies have been proposed, as pressure retarded osmosis (PRO) [11–13], reverse electrodialysis (RED) [14–17], and capacitive mixing (CAPMIX) [18–21], to harvest energy from salinity gradients. PRO is based on the osmosis effect through hydrophobic membranes, whose driven force originates from aqueous solutions with different concentrations, to produce net water flow, thus to generate electricity by means of a hydro-turbine. RED associates particular membranes which allow specified ions to proliferate across, forced by concentration gradients. Meanwhile electricity is produced with the ionic flow transformed into electrical current via imposed external circuits by redox reactions. CAPMIX is a capacitor through which different salt solutions alternatively flows, thus to provide electricity by charging and discharging under different capacitance with external electric circuits [22,23].

The salty aqueous solution in the above salinity gradient harvesting devices can be prepared by dissolving inorganic or thermolytic salts, such as ammonia–carbon dioxide [24], switchable polarity solvents [25], sodium chloride [26], in water. In accord with heat recovery, the above thermolytic or inorganic salts could be easily separated through the apparatus driven by the thermal energy. For example, membrane distillation (MD) can be driven by the low temperature heat to produce low and high concentration solutions [27–29].

* Corresponding authors.
E-mail addresses: r_long@hust.edu.cn (R. Long), w_liu@hust.edu.cn (W. Liu).

http://dx.doi.org/10.1016/j.memsci.2016.10.035
Received 15 August 2016; Received in revised form 26 September 2016; Accepted 23 October 2016
Available online 26 October 2016

Nomenclature

A_{MD}	Membrane area in the MD module (m^2)
A_{RE}	Exchange area in the RED module (m^2)
A	Effective hydrated ion radius (pm)
C_i	Electrolyte concentration (in molality) of the NaCl solution in stream i (mol kg^{-1})
$c_{p,l}$	Specific heat capacity of the feed solution (kJ kg^{-1} $°C^{-1}$)
D_{NaCl}, D_{Water}	Diffusion constants of NaCl and water, respectively (m^2 s^{-1})
E_{cell}	Electromotive force of one cell (V)
F	Faraday constant (96485C mol^{-1})
f	Obstruction factor
$h_L(C, T)$	Specific enthalpy of NaCl solution (of concentration C) at temperature T(kJ kg^{-1})
$h_{vap}(C, T)$	Specific enthalpy of vaporization of an NaCl solution (of concentration C) at temperature T (kJ kg^{-1})
I	Ion strength of a solution (mol L^{-1})
j	Current density (A m^2)
J	Flux of the salt or water (mol s^{-1} m^{-2})
$K_{m,MD}$	Mass transfer coefficient in the MD module (kg m^{-2} min^{-1} $°C^{-1}$)
$K_{c,RE}$	Heat transfer coefficient in the RED module (W m^{-2} $°C^{-1}$)
L_{MD}, L_{RE}	Lengths of the MD module and the RED module, respectively (m)
m_i	Mass flow rate of stream i (kg min^{-1})
Δm_{MD}	Change in the mass flow rate of the feed solution in the MD module (kg min^{-1})
m_F, m_P	Mass flow rates of the feed and the permeate streams in the MD module, respectively (kg min^{-1})
M_{H_2O}	Mole mass H_2O (0.01802kg mol^{-1})
P_{max}	Power (W)
p_w	Pressure (Pa)
Q_H	Heat absorbed from the heat source (W)
R	Gas constant (8.314J mol^{-1} K^{-1})
R_{AEM}, R_{CEM}	Area resistance of the AEM and CEM, respectively (Ω m^2)
R_a	Area resistance (Ω m^2)
S_i	Stream i
T_i	Temperature of stream i (°C)
T_H, T_C	Temperatures of the heat source and heat sink, respectively (°C)
T_H*, T_C*	Temperature of the pure permeate solution having the same partial vapor pressure (p_w) as the salty feed solution at T_H and T_C, respectively (°C)
T_F, T_P	Temperatures of the feed and permeate streams in MD, respectively (°C)
ΔT_{th}	Threshold temperature difference (°C)
T_h, T_c	Temperatures of the hot and the cold stream in RED, respectively (°C)
V_{HC}, V_{LC}	Volume flow rates of the HC and LC solution in the RED module (m^3 s^{-1})
W, L	The width and length of the RED membrane (m)
x	Axial position along the MD or RED module (m)
z	Valency of an ion

Greek Symbols

α	Relative MD permeate/feed solution flow rate; Permselectivity of the ion-selective membrane in RED module
β	Specific heat duty (J kg^{-1})
γ	Activity coefficient
δ_m	Membrane thickness (m)
δ_{HC}, δ_{LC}	Thickness of the HC and LC solution compartment, respectively (m)
η	Efficiency
Λ_m	Molar conductivity (S m^2 mol^{-1})
ρ_{H_2O}	Density of water (kg m^{-3})
ψ	Power per unit mass flow rate (J kg^{-1})
ξ	Mass recovery rate

Subscripts

HC	High concentration
LC	Low concentration
ext	External load
coul	Coulombic
cit	Co-ion transport
max	Maximum
min	Minimum

Abbreviations

MD	Membrane distillation
RED	Reversed electrodialysis
PRO	Pressure retarded osmosis
CAPMIX	Capacitive mixing
RE	Regenerator
CEM	Cation-exchange membrane
AEM	Anion-exchange membrane
IEM	Ion-exchange membranes
PLR	Permit limiting regime
FLR	Feed limiting regime
MTLR	Mass transfer limited regime

To maintain the stability and salt solution availability of the open-loop PRO system, closed-loop energy utilization systems based on PRO have been conceived, namely the MD-PRO system, where MD is employed during the thermal separation procedure to offer high and low concentration streams, and PRO is employed to extract useful work from the energy of mixing solutions with different concentrations [30,31]. In above existing MD-PRO systems, aqueous thermolytic salty aqueous solution (NaCl-water) and lithium chloride-methanol (LiCl-methanol) solution have been adopted as the working substance. These systems may be economically portable to harvest geothermal energy or waste heat from civil and industrial exhausts [30].

In this study, we put forward a novel hybrid electricity generation system employing MD for working solutions regeneration and RED for electricity generation, which uses NaCl dissolved in water as the working substance. The investigation was performed, to begin with by analyzing the performance of MD module during the thermal separation procedure, where streams with different NaCl concentrations were produced, driven by the low temperature heat source, and then by illustrating the electricity generated in the RED module that harvests the Gibbs free energy of mixing from the produced salty streams. The electrical efficiency of this proposed hybrid electricity generation system was modeled and calculated by considering both the heat and mass transfer characteristics during the thermal separation and electricity generation procedures. Major factors that determine the performance were systematically analyzed. Finally, the implications and feasibility of the proposed low-grade heat harvesting system were evaluated and discussed.

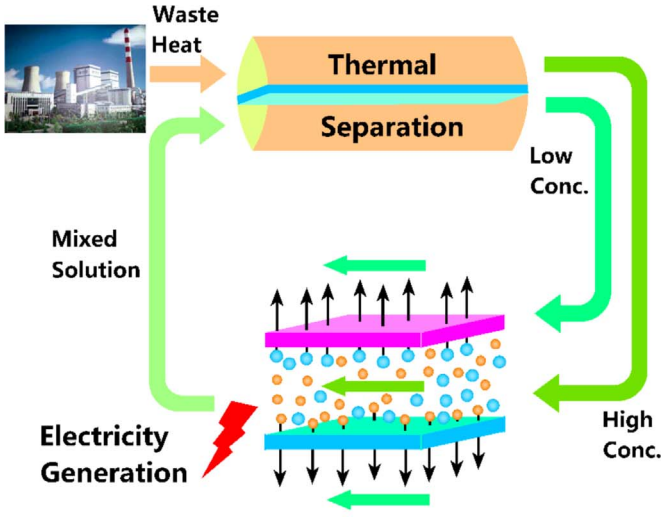

(a)

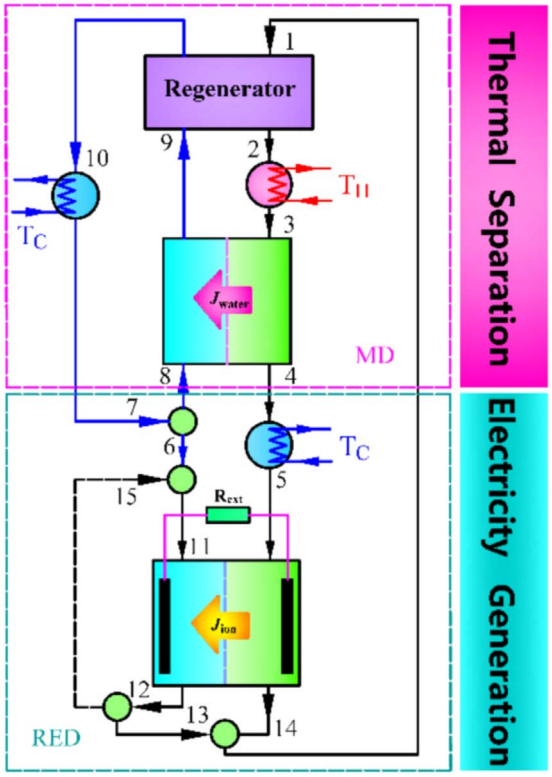

(b)

Fig. 1. Diagrammatic sketch of the proposed MD-RED hybrid electricity generation system to harvest low-grade thermal energy. This system includes the thermal separation section composed of a direct contact membrane distillation along with a regenerator, and the electricity generation section (reverse electrodialysis, RED for short). In the thermal separation section, driven by the low temperature heat source, streams with different NaCl concentrations are produced. In the electricity generation section, RED module harvests the Gibbs free energy of mixing from the produced salty streams to generate electricity. The stream i is denoted as S_i for convenience. Three streams (S_1, S_5, and S_6) bridge the thermal separation and electricity generation stages. Stream S_1 out of the RED module comes into the MD module with regenerator, thereby higher concentration solution (S_5) is generated. Another stream (S_6) originates from the open loop of permeate solution (S_7, S_8, S_9 and S_{10}). Streams S_5 and S_6 run into the RED module, then converge into stream S_1, meanwhile electricity is generated. (For interpretation of the references to color in this figure, the reader is referred to the web version of this article).

2. Model development and system description

A diagrammatic sketch of the proposed hybrid low-grade energy recovery system is depicted in Fig. 1. In this system, MD is adopted for the thermal separation of the salty aqueous solution and RED for electricity generation propose. The RED stack is composed of repeating pairs of ion-exchange membranes (IEMs) (cation-exchange membrane (CEM) and anion-exchange membrane (AEM)), and solutions with different concentrations alternatively flow through the channels between the IEMs [32,33]. The salt (NaCl solution in this paper) concentration gradient across the IEMs induces a Nernst potential. As counter-ions are selectively allowed to get through the IEMs, co-ions are remained while counter-ions diffuse from the high concentration (HC) compartment to the low concentration (LC) one. Cathode and anode are placed at the ends of the RED stack, and a redox couple is circulated between the end electrodes, thus electricity is generated by converting the ionic current to an electric current through the external circuit [34,35].

For convenience, we mark stream i as S_i with T_i, m_i, and C_i, respectively, representing its temperature, mass flow rate, and salinity. Three streams (S_1, S_5, and S_6) bridge the thermal separation and electricity generation stages, and the MD feed (S_1) NaCl concentration C_1 is defined as the working salinity of the proposed hybrid electricity generation system.

The solutions (S_{13} and S_{14}) out of the RED stack converge into S_1, which is afterwards separated through the MD module driven by thermal energy from the low-grade heat source (T_H) to engender concentrated stream (S_4). In order to decrease the energy needed in the thermal separation procedure and augment its energy efficiency, a regenerator is placed before the MD module to recover the latent heat accumulated in the permeate stream (S_9). A small part of effluent solution of the RED, S_{15}, is cycled to the influent, then mixed, to enhance the electrical conductivity of the pure water, thereby maintaining the stability of the RED.

On the system level, the proposed hybrid electricity generation system absorbs thermal energy from the external low-grade heat source (via red heat exchanger in Fig. 1), parts of which is converted to electricity, and the remaining is evacuated to the heat sinks (through two blue heat exchangers in Fig. 1). This MD-RED hybrid system has the heat-to-work characteristics of a generic heat engine, whose working mechanism will be explicated through exploiting the thermal separation procedure that consists of the MD module along with a regenerator (RE), and then illustrating the electricity generation procedure (electricity is generated by RED stacks).

2.1. Thermal separation procedure

S_3 and S_7 with temperatures T_3 and T_7, respectively, in thermal equilibrium with the heat source (T_H) and heat sink (T_C) enter the counter-flow MD module, where the temperature difference aside the hydrophobic membrane leads to an unequal partial vapor pressure, inducing a water vapor flux from the low concentration solution (feed solution) to the higher one (permeate solution). This trans-membrane water vapor flux Δm_{MD} is equivalent with the decrease of mass flow rate of the feed solution (from m_3 to m_4). For the open loop of permeate solution (S_7, S_8, S_9 and S_{10}), the input mass flow rate is the vapor flux Δm_{MD} which permeates across the hydrophobic membrane, and the output mass flow rate of the permeate loop is S_6. Hence, due to the mass balance, the requirement of steady state operation should meet that $\Delta m_{MD} = m_6$. The mass recovery rate, ξ, can be defined as the percentage of the water vapor flux across the hydrophobic membrane on the inlet flow rate of the feed solution [29]:

$$\xi = \Delta m_{MD}/m_3 = m_6/m_3 \quad (1)$$

Furthermore, another criterion evaluating the performance of the MD module in the thermal separation procedure can be characterized

by the energy efficiency. Here we use a recently defined parameter: specific heat duty (β) instead, indicating the ratio between heat required and the water vapor flux across the hydrophobic membrane [29].

$$\beta = \frac{Q_H}{\Delta m_{MD}} = \frac{c_{p,l}(T_3 - T_2)}{\xi} \tag{2}$$

where Q_H is the heat absorbed from the heat source, $c_{p,l}$ is the average specific capacity of feed solution S_2 in the hot heat exchanger. A regenerator is placed before the MD module to retrieve the latent heat accumulated in the outlet (S_9) of the permeate stream, thus to augment the MD energy efficiency, denoted as specific heat duty, in the thermal separation procedure by decreasing the temperature difference between T_3 and T_2. Moreover, another operating parameter, $\alpha = m_8/m_1$, can also be defined as the relative inlet permeate/feed solution mass flow rates in the MD [29], which is a key parameter that impacts the performance specifications of the hybrid electricity generation system, and will be discussed in detail in the following parts.

2.2. Modelling the heat and mass transfer characteristics in the MD and regenerator

According to the previous literatures [29], the control equations illustrating the heat and mass transfer characteristics in the direct contact MD are listed as below:

$$\frac{dm_F(x)}{dx} = \frac{A_{MD}}{L_{MD}} K_{m,MD}[T_F(x) - T_P(x) - \Delta T_{th}(x)] \tag{3}$$

$$\frac{dm_P(x)}{dx} = \frac{A_{MD}}{L_{MD}} K_{m,MD}[T_F(x) - T_P(x) - \Delta T_{th}(x)] \tag{4}$$

$$\frac{d[m_F(x)h_L(C(x), T_F(x))]}{dx} = \frac{dm_F(x)}{dx}[h_{vap}(C(x), T_F(x)) + h_L(0, T_F(x))] \tag{5}$$

$$\frac{d[m_P(x)h_L(0, T_P(x))]}{dx} = \frac{dm_P(x)}{dx}[h_{vap}(0, T_P(x)) + h_L(0, T_P(x)) + c_{p,V}(T_F(x) - T_P(x))] \tag{6}$$

The definitions of the variables used in these equations are given in the nomenclature at the end of this paper. Eqs. (3) and (4) are for the mass transfer driven by the partial vapor pressure difference induced by the temperature difference. For simplicity, the conductive heat transfer is negligible, hence Eqs. (5) and (6) are for the heat transfer, dominated by the convective transfer of vapor that carries the enthalpy through the microporous membrane. The boundary conditions for above equations are given by:

$$T_F(L_{MD}) = T_3 \tag{7}$$

$$m_F(L_{MD}) = m_1 \tag{8}$$

$$T_P(0) = T_8 \tag{9}$$

$$m_P(0) = \alpha m_1 \tag{10}$$

The distributions of the mass flow rate and temperature along the membrane can be calculated by solving the governing mass and heat transfer Eqs. (3)–(6), with the boundary conditions (Eqs. (7)–(10)).

There is no mass exchange in between the hot and cold streams in the regenerator. According to the energy balance, the governing equations for heat transfer in the regenerator are [29]:

$$m_9 \frac{dh_L(0, T_h(x))}{dx} = K_{c,RE} \frac{A_{RE}}{L_{RE}}[T_h(x) - T_c(x)] \tag{11}$$

$$m_1 \frac{dh_L(C_1, T_c(x))}{dx} = K_{c,RE} \frac{A_{RE}}{L_{RE}}[T_h(x) - T_c(x)] \tag{12}$$

The definitions of the variables used in these equations are given in the nomenclature at the end of this paper. The boundary conditions for Eqs. (11) and (12) are:

$$T_h(L_{RE}) = T_9 \tag{13}$$

$$T_c(0) = T_1 \tag{14}$$

The distributions of the temperature along the regenerator can be calculated by solving the governing heat transfer Eqs. (11) and (12), with the boundary conditions (Eqs. (13) and (14)).

2.3. Electricity generation procedure

Streams S_5 and S_6 with different concentrations of NaCl enter the RED module. In order to enhance the electrical conductivity of the solution on the low concentration side, a rather small amount of effluent of the RED (S_{15}) is cycled to the influent to enhance its concentration. The voltage of the reverse electrodialysis (RED) which stems from the Nernst potential difference across the cation exchange membrane (CEM) and the anion exchange membrane (AEM) is [36]

$$E_{cell}(x) = \alpha_{CEM} \frac{RT}{F} \ln \frac{\gamma_{HC}^{Na}(x) C_{HC}(x)}{\gamma_{LC}^{Na}(x) C_{LC}(x)} + \alpha_{AEM} \frac{RT}{F} \ln \frac{\gamma_{HC}^{Cl}(x) C_{HC}(x)}{\gamma_{LC}^{Cl}(x) C_{LC}(x)} \tag{15}$$

where α is the permselectivity of the membrane. γ is the activity

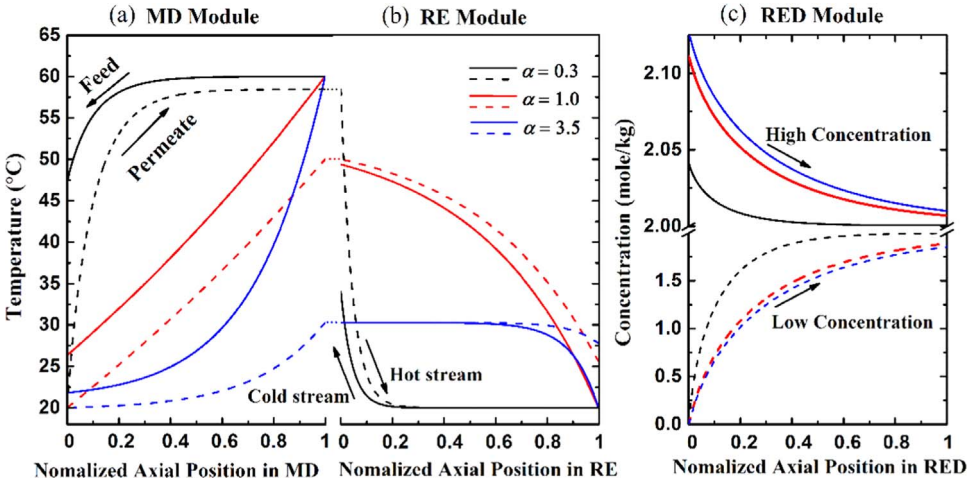

Fig. 2. Temperature profiles of the permeate and feed solutions in the MD (a), regenerator (RE) (b), and the concentration profiles in the RED (c) for different relative flow rates. At the outlet of the MD, the permeate solution (S_9) flows into the regenerator to heat up the cold stream (S_1). Hence the temperature of the permeate effluent is equivalent to that of the hot stream in the regenerator, which is denoted by the dash connecting lines. On the other hand, the streams out of the thermal separation procedure with different concentrations then goes into the RED module. By exchanging ions across the ion-selective membrane, the concentrations of the streams vary along the RED module.

coefficient. C is the concentration in mol/m^3.

Activity coefficients depend on the cell position and can be calculated with the extended Debye-Huckel equation [37]:

$$\gamma(x) = \exp\left[\frac{-0.51z^2\sqrt{I(x)}}{1 + (A/305)\sqrt{I(x)}}\right] \tag{16}$$

where I is the ion strength of the solution (mol/L). A is the effective hydrated ion radius ($A_{Na^+} = 450$ pm and $A_{Cl^-} = 300$ pm).

For a real-life RED system, the stack components are not ideally conductive but holds resistance that hinders the ionic and electric currents. For the one repeating RED cell, the space-dependent area specific resistance $R_{a,cell}(x)$ is [36,37]:

$$R_{a,cell}(x) = \frac{f}{\Lambda_m}\left(\frac{\delta_{HC}}{C_{HC}(x)} + \frac{\delta_{LC}}{C_{LC}(x)}\right) + R_{AEM} + R_{CEM} \tag{17}$$

where Λ_m is the molar conductivity of NaCl solution. δ_{HC} and δ_{LC} is the thickness of the HC and LC solution compartment. f is a measure for the increase of the electrical resistance due to the negative effects of the spacer. R_{AEM} and R_{CEM} are the membrane area resistance.

The space-dependent current density (j) can be calculated with Ohm's law

$$j(x) = \frac{E_{cell}(x)}{R_{a,cell}(x) + R_{a,ext}(x)} \tag{18}$$

Salt transport from the high concentration electrolyte to the low concentration electrolyte consists of a Coulombic part and the other part originating from co-ion transport [37]:

$$J_{total}(x) = J_{Coul}(x) + J_{cit}(x) = \frac{j(x)}{F} + \frac{2D_{NaCl}}{\delta_m}[C_{HC}(x) - C_{LC}(x)] \tag{19}$$

In addition, owing to the osmosis effect, there exists a water flux (J_{water})from the LC solution to the HC solution compartment. The volume water flux due to Osmotic affects is [38]

$$J_{water}(x) = -\frac{2D_{Water}}{\delta_m}[C_{HC}(x) - C_{LC}(x)]\frac{M_{H_2O}}{\rho_{H_2O}} \tag{20}$$

According to the previous literatures, the governing equations of the RED module are given by [37]

$$\frac{dC_{HC}(x)}{dx} = -\frac{W}{V_{HC}}J_{total}(x) - C_{HC}(x)\frac{WJ_{water}(x)}{V_{HC}} \tag{21}$$

$$\frac{dC_{LC}(x)}{dx} = \frac{W}{V_{LC}}J_{total}(x) + C_{LC}(x)\frac{WJ_{water}(x)}{V_{LC}} \tag{22}$$

For maximum power of the RED cell, the external load should be equal to the internal resistance, therefore, the space-dependent external load ($R_{a,ext}(x)$) takes the value of $R_{a,cell}(x)$. Hence the space-dependent power density is given by

$$P_{d,\,max}(x) = \frac{1}{2}j(x)^2R_{a,u}(x) \tag{23}$$

The total maximum power output is

$$P_{max} = W\int_0^L P_{d,\,max}(x)dx \tag{24}$$

where W and L are, respectively, the width and length of the RED membrane.

Furthermore, for small molarities of the salt solution, the concentration change does not obviously impact the density of the solutions, and the osmosis of water from the LC solution to the HC solution compartment is quite weak. The volume flow rates (V_{LC} and V_{HC}) in the

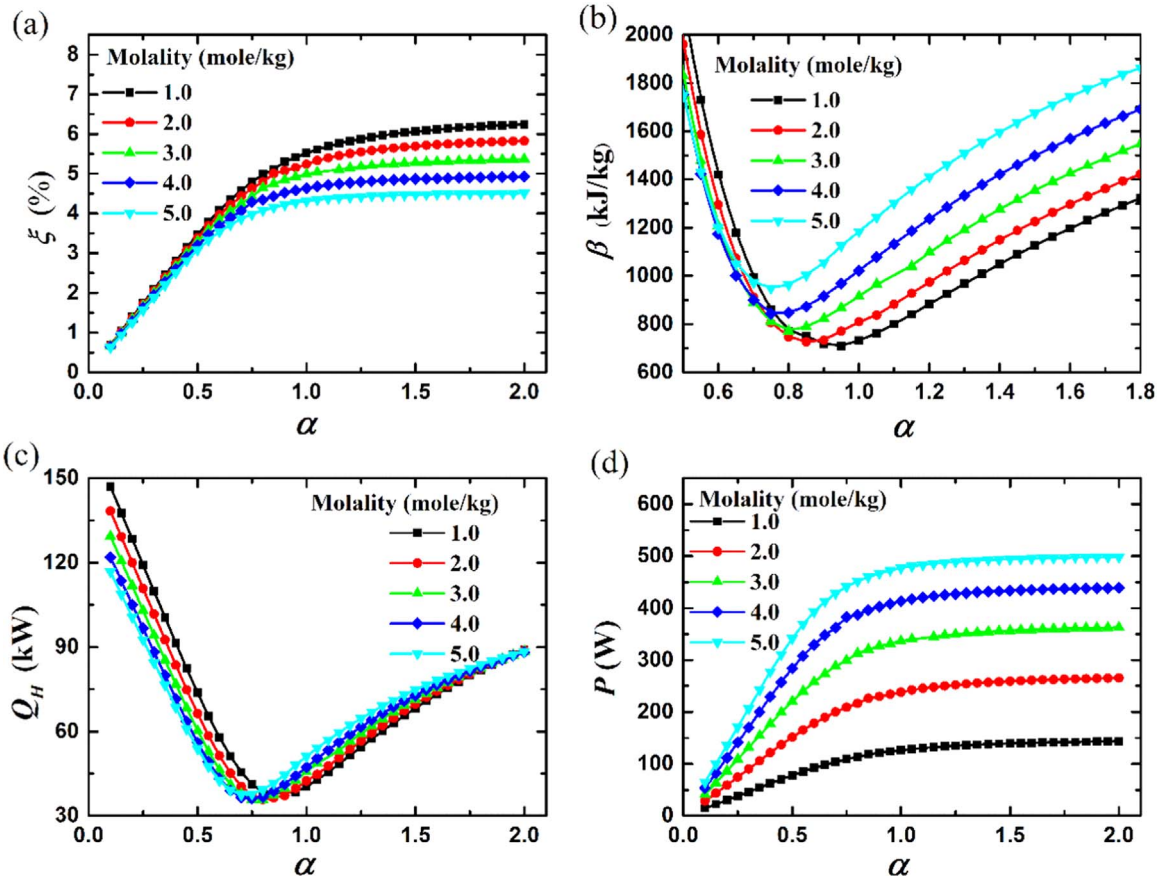

Fig. 3. Simulations of the hybrid MD-RED system for given heat and mass transfer coefficients with NaCl molarities being 1.0, 2.0, 3.0, 4.0, and 5.0 mol/kg in the MD feed stream. Mass recovery rate (a), specific heat duty (b), heat absorbed (c), and power output (d) vary with the relative MD permeate/feed solution flow rate. In these model simulations, the heat sink and source temperatures are, respectively, fixed at 20 °C and 60 °C.

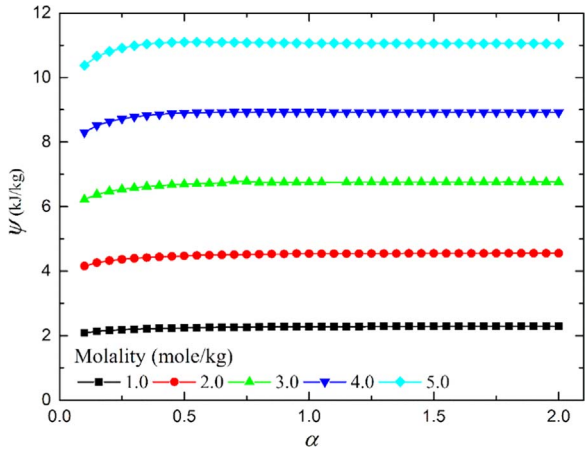

Fig. 4. Solution unit work potential ($\psi(C_1)$) varies with the relative MD permeate/feed solution flow rate.

RED module can be treated as constants. Therefore Eq. (24) can be rewritten as

$$P_{max} \approx m_5 \psi(C_1) = m_1 \xi \psi(C_1) \tag{25}$$

where $\psi(C_1)$ is denoted as the power per unit mass flow rate of the salty solution, and has the dimension of J/kg. It is can be treated as unit work potential of the solutions, which will be discussed numerically in the following text.

2.4. Electrical efficiency of the hybrid electricity generation system

Detailed analysis of the aforementioned thermal separation and electricity generation procedures indicates that the hybrid electricity generation system absorbs an amount of thermal energy (Q_H) and then generates electricity (P_{max}). Hence, this hybrid electricity generation system has the heat-to-work characteristics of a generic heat engine, whose electrical efficiency, η, can be expressed as:

$$\eta = \frac{P_{max}}{Q_H} \approx \frac{\psi(C_1)}{\beta} = \frac{\xi \psi(C_1)}{c_{p,l}(T_3 - T_2)} \tag{26}$$

3. Performance analysis of the hybrid electricity generation system

3.1. System process configuration

To start with, the temperature profiles along the normalized axis poison in the MD and the regenerator, and the concentration profiles in the RED module for different relative flow rates are depicted in Fig. 2. These temperature or concentration profiles present different characteristics under different relative flow rates. The permeate solution absorbs heat from the feed solution in the MD module, then heat up the effluent solution from the RED module in the regenerator. Previous literatures about the MD with regenerator shed light on that the main performance specifications (ξ and β) are mainly impacted by the relative flow rate α [29], which, in consequence, influences the performance of the RED module. There exist three operating condition of the MD-RE module, which can be categorized as permit limiting regime (PLR) at small α, feed limiting regime (FLR) at large α, and mass transfer limited regime (MTLR) at moderate α [29]. In the PLR, the permeate solution is insufficient. Due to the mechanism of MD process, the permeate solution increases from T_C to T_H* where T_H* can be calculated by solving the equation $p_w(0, T_H^*) = p_w(C_F, T_H)$, with C_F being the feed solution concentration, which is shown in Fig. 2(a) for $\alpha = 0.3$. In the FLR, the feed solution is insufficient. The driving force of MD process vanishes, and the feed solution drops from T_H to T_C*, where T_C^* can be calculated by solving the equation $p_w(0, T_C) = p_w(C_F, T_C^*)$, which is shown in Fig. 2(a) for $\alpha = 3.5$. When the trans-membrane mass coefficient or the hydrophobic membrane area is not larger enough, the temperature of the permeate solution could not increase to T_H*, and that of the feed solution could not drop to T_C*. This is the MTLR as shown in Fig. 2(a) for $\alpha = 1$. Furthermore, as illustrated in Fig. 2(b), the insufficient permeate or feed solution in the PLR or FLR leads to limited heat transfer in the regenerator (RE), and the MTLR results in unlimited heat transfer in the RE.

Larger α means larger mass flow rate of the permeate solution, therefore lower temperature rise in the MD module and lower temperature decrease in the regenerator, hence a larger feed solution concentration at the effluent of the MD module according to the mechanism of the MD process, as shown in Fig. 2(c), where the influent solution of high concentration in RED originates from the effluent feed solution in the MD module. In the RED module, the solution concentrations of two different solutions vary to the moderate ones: the higher concentration drops while the lower concentration increases by exchanging ions through the RED membrane.

3.2. Key performance parameters of the hybrid electricity generation system

The relative MD permeate/feed solution flow rate plays a determinative role on performance specifications of the thermal separation procedure, which mainly are mainly reflected by mass recovery rate (ξ), heat absorbed (Q_H) and specific heat duty (β). In the analysis, the inlet mass flowrate of MD feed solution (S_1 in Fig. 1) is fixed, while that of the permeate solution (S_8 in Fig. 1) varies under different relative MD permeate/feed solution flow rates. Numerical results suggests that ξ presents a linear monotonic increasing function with α at small values of α, then reaches a plateau ξ_{max} at higher values of α, which correspond to the permeate limiting regime (PLR) and the feed limiting regime (FLR), respectively, according to the aforementioned analysis, as depicted in Fig. 3(a). In Fig. 3(b), we can see that β has a minimum value as α increases. The higher molarity, the lower α that corresponds to the minimum value of specific heat duty (β_{min}), however, higher value of β_{min}. In Fig. 3(c), the heat absorbed in the MD process decreases with increasing α, reaches its minimum value, then increases for different MD feed NaCl concentrations. Furthermore, the heat absorbed in the thermal separation stage is $Q_H = m_1 c_{p,l}(T_3 - T_2)$, where $c_{p,l}$ is the average specific capacity of feed solution S_2 in the hot heat exchanger. The impact of different molality of MD feed solution on the average specific capacity of the stream is not so obvious under the studied operation conditions. Therefore, the difference of heat absorbed under different molality for a given relative MD permeate/feed solution flow rate is not big. In the FLR, due to the unlimited mass

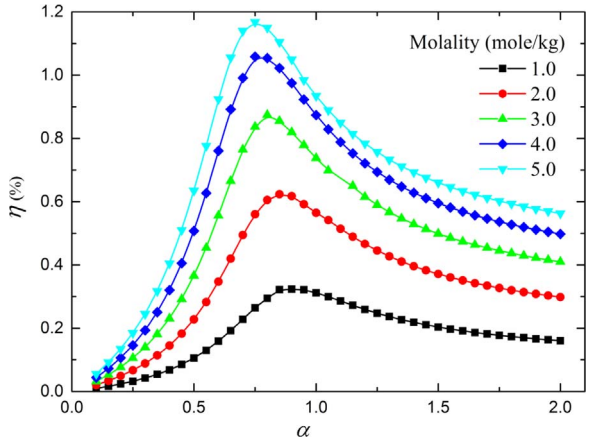

Fig. 5. Electrical efficiency of the MD-RED system varies with the relative MD permeate/feed solution flow rate.

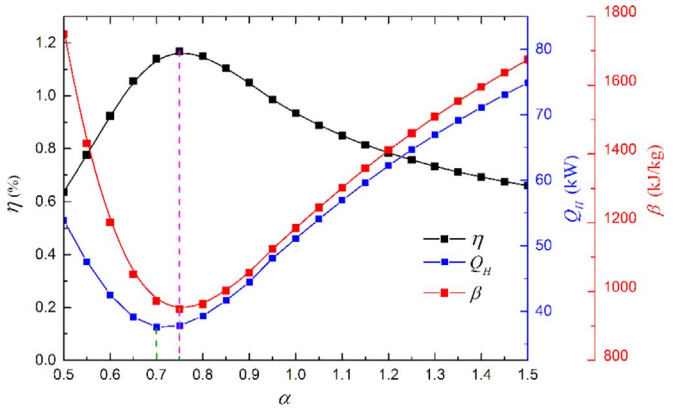

Fig. 6. Heat absorbed, specific heat duty, and electrical efficiency of the hybrid MD-RED system vary with the relative flow rate for MD feed stream NaCl concentration of 5.0 mol/kg.

transfer, the heat absorbed under different molarities coincide with each other at higher relative flow rates. The higher molarity, the lower αcorresponding to the minimum heat absorbed. In Fig. 3(b) and (c), we can see that the optimal relative flow rate corresponding to the minimum specific heat duty shows a slight difference from that corresponding to the minimum heat absorbed. Furthermore, in Fig. 4, we have that $\psi(C_1)$ is nearly independent of the relative flow rate α when α is not very small. Therefore for the most conditions $\psi(C_1)$ can be treated as a constant merely determined by the MD feed NaCl concentration for given temperatures. According to Eq. (25), $P_{\max} \approx m_1 \xi \psi(C_1)$, which demonstrates the power output should exhibit same behaviors as the ξ for a given MD feed concentration. It increases linearly with increasing α in the PLR, then reaches a plateau at higher values of α in the FLR, which can also be seen in Fig. 3(d). However, the impact of the MD feed NaCl concentration on the RED power output presents different behaviors, compared with that on the trends of the mass recovery rate. Larger MD feed NaCl concentration induces more power output. Despite a higher concentration of the MD feed solution results in lower mass recovery rate which means a smaller NaCl concentration rise after the MD process, the initial concentration is sufficient enough to maintain a lager voltage of the reverse electrodialysis (RED) based on Eq. (15). Therefore, the higher molarity of the concentration, the larger power output.

3.3. Overall electrical efficiency of the hybrid electricity generation system

After the heat absorbed and power output are obtained, the electrical efficiency can be readily calculated, which is illustrated in Fig. 5. The curve of electrical efficiency and relative MD permeate/feed solution flow rate α is concave under different molarities. There exists an optimal α leading to the maximum electrical efficiency, which corresponds to the minimum value of specific heat duty, rather than the minimum heat absorbed during the thermal separation procedure as shown in Fig. 6. We can also see that a higher concentration of the MD feed solution induces a higher specific duty, and a higher electrical efficiency, because of the fact that the favorable influence of a higher voltage of the reverse electrodialysis (RED) on the electrical efficiency overrides the negative influence of a larger β, which means more thermal energy required by the MD module during the thermal separation procedure.

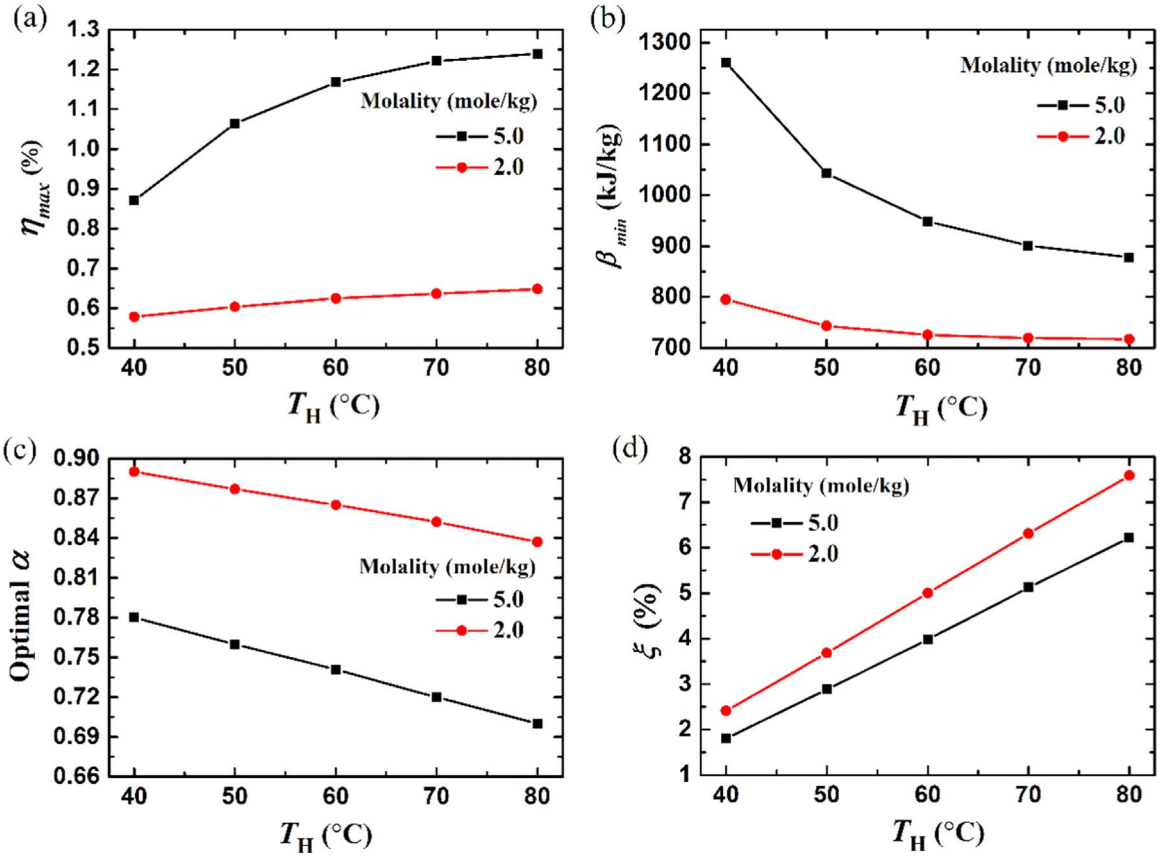

Fig. 7. Maximum electricity efficiency η_{max} (a), Minimum specific heat duty β_{min} (b), Optimal relative MD permeate/feed solution flow rate (c), and Mass recovery rate (d) of the hybrid MD-RED system as a function of the heat source temperature under given heat and mass transfer coefficient with NaCl molarities of 2.0 and 5.0 mol/kg in MD feed solution. In the calculations, the temperature of the heat sink is fixed at 20 °C.

4. Thermodynamic limits of the electrical efficiency

According to the aforementioned analysis, there exists a maximum electrical efficiency, which corresponds to the minimum specific heat duty , and the optimal relative flow rate. For given operation temperatures, based on Eq. (26), we have

$$\eta_{max} \approx \frac{\psi(C_1)}{\beta_{min}} \tag{27}$$

Similar to the aforementioned analysis, the performance specifications of the MD-RED system with different NaCl molarities of 2.0 and 5.0 mol/kg in MD feed solution are investigated. Fig. 7(a) shows the relation between maximum electrical efficiency η_{max} and T_H for a given T_C (20 °C). The maximum electrical efficiency augments with increasing T_H, as it is often the case that larger heat source temperature means larger average temperature of the working substance in the heat absorbing process, thus resulting higher electrical efficiency of the proposed MD-RED system. It also reveals that the higher MD Feed NaCl concentration, the larger maximum electrical efficiency. The relation of minimum specific heat duty with the heat source temperature T_H is present in Fig. 7(b). We can see that the minimum specific heat duty (β_{min}) shows a decreasing function of T_H, but it increases with increasing MD feed NaCl concentrations, which is also depicted in Fig. 3(b). The optimal relative flow rate decreases with increasing heat source temperatures and MD feed concentrations. Larger MD feed NaCl concentrations leads to lower optimal α and the corresponding mass recovery rate as shown in Fig. 7(d), hence higher β_{min}, which presents great accordance with Eq. (2).

5. Conclusions and implications

The intrinsic low thermodynamic limitation (Carnot efficiency) and high energy losses hinder the efficient utilization of the low temperature heat source for electricity generation. Actually, for low temperature heat source utilization, it is more appealing to directly use its thermal energy for hot water supply, or for the industrial and agricultural drying process through heat exchangers. However, in remote areas, where direct thermal utilization is not applicable, the only feasible way is to convert it into electricity by heat engine cycles.

In present paper, a hybrid system consisting a MD module and RED module is investigated to harvest low temperature thermal energy. Electrical efficiency is a critical performance objective that affects the feasibility of the hybrid electricity generation system. In this paper, the electricity efficiency of the proposed hybrid system reaches 1.15% operating between 20 and 60 °C with the MD feed NaCl concentration of 5 mol/kg. Under the same operating temperature ranges, a charging-free aqueous electrochemical cell is adsorbed to harvest low-grade heat, whose efficiency reaches 1.2% with the regenerative efficiency being 50% [39]. Thermoelectric devices are also applied to directly convert temperature gradient into electricity. However the extremely low ZT value at the low temperatures render the application [40]. Here the proposed electricity generation system shows its advantage for potential utilization.

To step toward application, efforts should be focused on enhancing the performance of membrane-based MD and RED processes. The characteristics of membranes in the MD and RED facilities directly determine the overall electrical efficiency of the hybrid electricity system. And the electrolyte solutions should also be coupled and addressed. In addition, an experimental analysis of a sequential open-looped MD-RED subsystem for simultaneous production of desalted water and electrical energy was investigated by Tufa et al. [17], indicating the possibility to conduct an experiment on the proposed hybrid electricity generation system, thus to give a deep insight into its performance and application, which will be analyzed in our further research. Furthermore, combined CAPMIX with MD hybrid system could also be conceived to harvest low-grad heat. In the above technologies (PRO, RED, and CAPMIX) based on salinity differences, which could be produced by the MD process, the required heat could be supplied by the solar energy (i.e. via a solar concentrator [41]), waste heat from the civil and industrial exhausts, geothermal sources. In this sense, the techniques contribute to the clean and renewable energy utilization, and especially in remote areas. In addition, for further commercial applications, a detailed technoeconomic analysis should be conducted on the system scale to inform the economic viability of the proposed hybrid electricity generation system.

Acknowledgements

We acknowledge the support received from the National Key Basic Research Program of China (973 Program) (2013CB228302).

References

[1] M.Z. Jacobson, Energy modelling: clean grids with current technology, Nat. Clim. Change 6 (2016) 441–442.
[2] N.L. Panwar, S.C. Kaushik, S. Kothari, Role of renewable energy sources in environmental protection: a review, Renew. Sustain. Energy Rev. 15 (2011) 1513–1524.
[3] M. Hatami, D.D. Ganji, M. Gorji-Bandpy, A review of different heat exchangers designs for increasing the diesel exhaust waste heat recovery, Renew. Sustain. Energy Rev. 37 (2014) 168–181.
[4] J. Bao, L. Zhao, A review of working fluid and expander selections for organic Rankine cycle, Renew. Sustain. Energy Rev. 24 (2013) 325–342.
[5] X. Zhang, M. He, Y. Zhang, A review of research on the Kalina cycle, Renew. Sustain. Energy Rev. 16 (2012) 5309–5318.
[6] R. Long, Y.J. Bao, X.M. Huang, W. Liu, Energy analysis and working fluid selection of organic Rankine cycle for low grade waste heat recovery, Energy 73 (2014) 475–483.
[7] R. Long, B. Li, Z. Liu, W. Liu, Performance analysis of a thermally regenerative electrochemical cycle for harvesting waste heat, Energy 87 (2015) 463–469.
[8] R. Long, B. Li, Z. Liu, W. Liu, A hybrid system using a regenerative electrochemical cycle to harvest waste heat from the proton exchange membrane fuel cell, Energy 93 (2015) 2079–2086.
[9] R. Long, B. Li, Z. Liu, W. Liu, Performance analysis of a dual loop thermally regenerative electrochemical cycle for waste heat recovery, Energy 107 (2016) 388–395.
[10] R.E. Pattle, Production of electric power by mixing fresh and salt water in the hydroelectric pile, Nature 174 (1954) 660.
[11] K.L. Hickenbottom, J. Vanneste, T.Y. Cath, Assessment of alternative draw solutions for optimized performance of a closed-loop osmotic heat engine, J. Membr. Sci. 504 (2016) 162–175.
[12] A. Achilli, A.E. Childress, T.Y. Cath, Power generation with pressure retarded osmosis: an experimental and theoretical investigation, J. Membr. Sci. 343 (2009) 42–52.
[13] R.L. Mcginnis, J.R. Mccutcheon, M. Elimelech, A novel ammonia–carbon dioxide osmotic heat engine for power generation, J. Membr. Sci. 305 (2007) 13–19.
[14] D.A. Vermaas, M. Saakes, K. Nijmeijer, Power generation using profiled membranes in reverse electrodialysis, Fuel Energy Abstr. 385–386 (2011) 234–242.
[15] E. Güler, R. Elizen, M. Saakes, K. Nijmeijer, Micro-structured membranes for electricity generation by reverse electrodialysis, J. Membr. Sci. 458 (2014) 136–148.
[16] A.M. Weiner, R.K. Mcgovern, H.L.V. John, A new reverse electrodialysis design strategy which significantly reduces the levelized cost of electricity, J. Membr. Sci. 493 (2015) 605–614.
[17] A. Tufa, E. Curcio, E. Brauns, W. van Baak, E. Fontananova, G. Di Profio, Membrane distillation and reverse electrodialysis for near-zero liquid discharge and low energy seawater desalination, J. Membr. Sci. 496 (2015) 325–333.
[18] R.A. Rica, R. Ziano, D. Salerno, F. Mantegazza, M.Z. Bazant, D. Brogioli, Electro-diffusion of ions in porous electrodes for capacitive extraction of renewable energy from salinity differences, Electrochim. Acta 92 (2013) 304–314.
[19] F. Liu, O. Schaetzle, B.B. Sales, M. Saakes, C.J.N. Buisman, H.V.M. Hamelers, Effect of additional charging and current density on the performance of capacitive energy extraction based on Donnan potential, Energy Environ. Sci. 5 (2012) 8642–8650.
[20] D. Brogioli, R. Ziano, R.A. Rica, D. Salerno, O. Kozynchenko, H.V.M. Hamelers, F. Mantegazza, Exploiting the spontaneous potential of the electrodes used in the capacitive mixing technique for the extraction of energy from salinity difference, Energy Environ. Sci. 5 (2012) 9870–9880.
[21] R.A. Rica, R. Ziano, D. Salerno, F. Mantegazza, D. Brogioli, Thermodynamic relation between voltage-concentration dependence and salt adsorption in electrochemical cells, Phys. Rev. Lett. 109 (2012) 684–691.
[22] B. Sales, M. Saakes, J. Post, C. Buisman, P. Biesheuvel, H. Hamelers, Direct power production from a water salinity difference in a membrane-modified supercapacitor flow cell, Environ. Sci. Technol. 44 (2010) 5661–5665.
[23] F. La Mantia, M. Pasta, H.D. Deshazer, B.E. Logan, Y. Cui, Batteries for efficient energy extraction from a water salinity difference, Nano Lett. 11 (2011)

1810–1813.
[24] R.L. McGinnis, M. Elimelech, Global challenges in energy and water supply: the promise of engineered osmosis, Environ. Sci. Technol. 42 (2008) 8625–8629.
[25] M.L. Stone, C. Rae, F.F. Stewart, A.D. Wilson, Switchable polarity solvents as draw solutes for forward osmosis, Desalination 312 (2013) 124–129.
[26] A.P. Straub, N.Y. Yip, M. Elimelech, Raising the bar: increased hydraulic pressure allows unprecedented high power densities in pressure-retarded osmosis, Environ. Sci. Technol. Lett. 1 (2013) 55–59.
[27] T.C. Chen, C.D. Ho, H.M. Yeh, Theoretical modeling and experimental analysis of direct contact membrane distillation, J. Membr. Sci. 330 (2009) 279–287.
[28] V.A. Bui, L. Vu, M. Nguyen, Modelling the simultaneous heat and mass transfer of direct contact membrane distillation in hollow fibre modules, J. Membr. Sci. 353 (2010) 85–93.
[29] S. Lin, N.Y. Yip, M. Elimelech, Direct contact membrane distillation with heat recovery: thermodynamic insights from module scale modeling, J. Membr. Sci. 453 (2014) 498–515.
[30] S. Lin, N.Y. Yip, T.Y. Cath, C.O. Osuji, M. Elimelech, Hybrid pressure retarded osmosis–membrane distillation system for power generation from low-grade heat: thermodynamic analysis and energy efficiency, Environ. Sci. Technol. 48 (2014) 5306–5313.
[31] E. Shaulsky, C. Boo, S. Lin, M. Elimelech, Membrane-based osmotic heat engine with organic solvent for enhanced power generation from low-grade heat, Environ. Sci. Technol. 49 (2015) 5820–5827.
[32] J.N. Weinstein, F.B. Leitz, Electric power from differences in salinity: the dialytic battery, Science 191 (1976) 557–559.
[33] J. Veerman, M. Saakes, S. Metz, G. Harmsen, Reverse electrodialysis: performance of a stack with 50 cells on the mixing of sea and river water, J. Membr. Sci. 327 (2009) 136–144.
[34] J.G. Hong, Y. Chen, Nanocomposite reverse electrodialysis (RED) ion-exchange membranes for salinity gradient power generation, J. Membr. Sci. 460 (2014) 139–147.
[35] N.Y. Yip, D.A. Vermaas, K. Nijmeijer, M. Elimelech, Thermodynamic, energy efficiency, and power density analysis of reverse electrodialysis power generation with natural salinity gradients, Environ. Sci. Technol. 48 (2014) 4925–4936.
[36] J. Veerman, J. Post, M. Saakes, S. Metz, G. Harmsen, Reducing power losses caused by ionic shortcut currents in reverse electrodialysis stacks by a validated model, J. Membr. Sci. 310 (2008) 418–430.
[37] J. Veerman, M. Saakes, S.J. Metz, G.J. Harmsen, Reverse electrodialysis: a validated process model for design and optimization, Chem. Eng. J. 166 (2011) 256–268.
[38] J. Veerman, R. De Jong, M. Saakes, S. Metz, G. Harmsen, Reverse electrodialysis: comparison of six commercial membrane pairs on the thermodynamic efficiency and power density, J. Membr. Sci. 343 (2009) 7–15.
[39] Y. Yang, S.W. Lee, H. Ghasemi, J. Loomis, X. Li, D. Kraemer, G. Zheng, Y. Cui, G. Chen, Charging-free electrochemical system for harvesting low-grade thermal energy, Proc. Natl. Acad. Sci. 111 (2014) 17011–17016.
[40] G. Kim, L. Shao, K. Zhang, K.P. Pipe, Engineered doping of organic semiconductors for enhanced thermoelectric efficiency, Nat. Mater. 12 (2013) 719–723.
[41] R. Long, B. Li, Z. Liu, W. Liu, Performance analysis of a solar-powered solid state heat engine for electricity generation, Energy 93 (Part 1) (2015) 165–172.